

Article

Enhanced High-Rate Capability of Iodide-Doped $\text{Li}_4\text{Ti}_5\text{O}_{12}$ as an Anode for Lithium-Ion Batteries

Lukman Noerochim^{1,*}, Rachmad Sulaksono Prabowo², Widyastuti Widyastuti¹, Diah Susanti¹, Achmad Subhan³ and Nurul Hayati Idris⁴

¹ Department of Materials and Metallurgical Engineering, Sepuluh Nopember Institute of Technology, Surabaya 60111, Indonesia

² Department of Mechanical Engineering, University of Balikpapan, Pupuk Raya Rd, Gunung Bahagia, Balikpapan 76114, Indonesia

³ Research Center of Physics, Indonesian Institute of Science, Serpong 15314, Indonesia

⁴ Energy Storage Research Group, Faculty of Ocean Engineering Technology and Informatics, Universiti Malaysia Terengganu, Kuala Nerus 21030, Terengganu, Malaysia

* Correspondence: lukman@mat-eng.its.ac.id

Abstract: $\text{Li}_4\text{Ti}_5\text{O}_{12}$ (LTO) is an alternative anode material to substitute commercial graphite for lithium-ion batteries due to its superior long cycle life, small volume change (zero strain), good thermal stability, and relatively high power. In this work, iodide-doped LTO is prepared by solid-state reaction method via ball milling method and subsequently calcined at 750 °C for 10 h in air atmosphere. X-ray diffraction (XRD) of iodide-doped LTO reveals the spinel cubic structure without any impurities detected. The 0.2 mol lithium iodide-doped LTO shows enhanced high-rate capability with a specific discharge capacity of 123.31 mAh g⁻¹ at 15 C. The long cyclic performance of 0.2 mol lithium iodide-doped LTO delivers a specific discharge capacity of 171.19 mAh g⁻¹ at 1 C with a capacity retention of 99.15% after 100 cycles. It shows that the iodide-doped LTO is a promising strategy for preparing a high electrochemical performance of LTO for the anode of lithium-ion batteries.

Keywords: iodide; doping; $\text{Li}_4\text{Ti}_5\text{O}_{12}$; anode; lithium-ion batteries



Citation: Noerochim, L.; Prabowo, R.S.; Widyastuti, W.; Susanti, D.; Subhan, A.; Idris, N.H. Enhanced High-Rate Capability of Iodide-Doped $\text{Li}_4\text{Ti}_5\text{O}_{12}$ as an Anode for Lithium-Ion Batteries. *Batteries* **2023**, *9*, 38. <https://doi.org/10.3390/batteries9010038>

Academic Editor: Dong Liu

Received: 7 December 2022

Revised: 29 December 2022

Accepted: 3 January 2023

Published: 5 January 2023



Copyright: © 2023 by the authors. Licensee MDPI, Basel, Switzerland. This article is an open access article distributed under the terms and conditions of the Creative Commons Attribution (CC BY) license (<https://creativecommons.org/licenses/by/4.0/>).

1. Introduction

A conventional lithium-ion battery consists of a LiCoOx cathode and a graphite anode. The graphite has a theoretical capacity of 372 mAh g⁻¹. The lithium insertion in graphite occurs at a voltage lower than 0.1 V (vs. Li/Li⁺) [1]. The graphite will be polarized to form lithium dendrites that are highly active on the electrode surface at high discharge rates [2,3]. These dendrites easily penetrate into the separator pores, causing an electric short circuit. Therefore, it is necessary to develop alternative anode materials with high safety, good performance, and long cycle stability in high-power batteries.

Carbon-based materials, tin, and silicon have been studied as ideal anode materials for lithium-ion batteries [4,5]. These materials have a high theoretical capacity and broad working potential. On the other hand, these materials exhibit significant volume changes during the charge–discharge cycles, thus limiting their practical application. Other materials, such as transition-metal oxides (TiO₂, MoO₂, SnO₂, etc.), were investigated for lithium-ion batteries with high energy density [6]. However, transition-metal oxides experience high initial irreversible discharge capacity and poor cycle capability at high-rate current density. High specific capacity and rate capabilities have been demonstrated by phosphorene-based anode materials in lithium-ion batteries [7]. It is reported that the exfoliated phosphorene in acetone had initial capacities of 1732 and 545 mAh g⁻¹ at 100 mA g⁻¹, respectively. The rate capability performance has a specific capacity of 345 and 200 mAh g⁻¹ for the exfoliated phosphorene in acetone at 1 Ag⁻¹. However, the significant volume expansion of

phosphorene is what causes the enormous capacity fading that was observed after 20 cycles (480 and 250 mAh g⁻¹). It is the biggest challenge for phosphorene-based anode materials for lithium-ion battery application.

Titanium-based compounds such as Li₄Ti₅O₁₂ (LTO) are attracting attention as alternative anodes for high-power lithium-ion batteries. Compared to graphite, LTO has a three-dimensional crystal lattice that supports the insertion/separation of Li⁺ ions, and LTO has a higher working voltage (about 1.5 V vs. Li/Li⁺) in the potential window of 1.2–4.3 V [8,9]. In addition, LTO has low polarization at high current levels and negligible lattice strain (volume change equal to 0.2%, significantly lower than that of graphite) during lithiation/delithiation [10,11]. These characteristics lead to good cycling capability as the anode of lithium-ion batteries. Recent studies of LTO reported that lithium-ion batteries had shown good safety even at fast charging rates above 20 C [12,13]. However, such anodes have certain drawbacks which are manifested in some of the lower battery energy densities [14].

LTO has low electronic conductivity and poor lithium-ion diffusion, so it limits its performance at high rate levels [15]. The specific capacity of LTO is also relatively low (the theoretical value is 175 mAh g⁻¹) [16]. In addition, the relatively high redox potential of LTO also reduces the potential window and weakens the energy storage performance of lithium-ion batteries [17].

Several strategies have been carried out to improve the electrochemical properties of LTO in recent years. Incorporating metal ions or atoms (Na⁺, Mg²⁺, Ca²⁺, Zn²⁺, Cu²⁺, La³⁺, Al³⁺, Cr³⁺, Mn⁴⁺, Nb⁵⁺, W⁶⁺) into LTO crystals can improve performance in high-rate lithium-ion batteries due to increased electronic conductivity [18–27]. However, some of the preparation and synthesis methods are time consuming, high cost, and requiring complicated equipment which prevents them from being used in commercial applications. Furthermore, this strategy distorts the LTO crystal, resulting in the loss of the zero-strain characteristic to a certain extent so that the battery life is reduced [28]. Doping non-metal ions (F⁻ and Br⁻) is also expected to be an effective way to optimize the electrochemical properties of LTO anode materials [29]. It is reported that fluoride-doped LTO with Li₄Ti₅O_{12-x}F_x (0 ≤ x ≤ 0.5) has improved rate capability when x = 0.174 [30]. The electronic conductivity of fluoride-doped LTO increased through Ti³⁺ generation delivering high-rate capability of 144, 123, 108, 91, and 60 mAh g⁻¹ at 5, 10, 30, 60, and 140 C, respectively. Doping bromide to LTO structure has enhanced the electronic conductivity and increased Li⁺ diffusion coefficient of Li₄Ti_{5-x}W_xO_{12-x}Br_x (x = 0.025, 0.050, 0.100) [31]. Doping F⁻ and Br⁻ is expected to replace the oxygen anion site (32e) on the octahedral site of spinel cubic structure promoting Ti³⁺ formation in the lattice, thereby increasing the electron concentration in the bulk.

In a previous study, we successfully synthesized the fluoride-doped LTO using a solid-state reaction [32]. The F⁻ anion added to the LTO contributes a good discharge capacity of 172 mAh g⁻¹ at 0.5 C, close to the theoretical capacity (175 mAh g⁻¹). F-doped LTO through solid-state reactions showing improved electrochemical performance. The F⁻ anion added to LTO can increase the electronic conductivity of LTO [33]. However, these anode materials still experienced severe degradation at high-rate performance. In addition to fluoride and bromide as a dopant for oxygen site, iodide was selected as alternative doping for LTO based on previous results showing successfully enhanced conductivity of various materials such as TiO₂ [34], carbon nanotubes [35], polyaniline [36], etc. As far as we know, iodide doping for LTO is still rarely explored, therefore there are still wide opportunities to investigate by simple preparation method the phenomena occurring due to iodide doping, especially in LTO as the anode of lithium-ion batteries.

In this work, iodide-doped LTO was synthesized through a solid-state route by ball milling, followed by calcination at a high temperature of about 750 °C for several hours. The effect of iodide doping on crystal structure and electrochemical performance has been systematically investigated. The 0.2 mol lithium iodide-doped LTO exhibits highly improved rate capability and cycling performance compared to pristine LTO.

2. Results

The XRD pattern of pristine LTO and iodide-doped LTO calcined at 750 °C for 10 h are shown in Figure 1a. According to JCPDS card No. 49-0207, the peaks of the XRD were completely identified as lithium titanate spinel structure. In all of the iodide-doped LTO samples, no impurity can be detected. With increasing iodide doping, the intensity peaks of iodide-doped LTO increase.

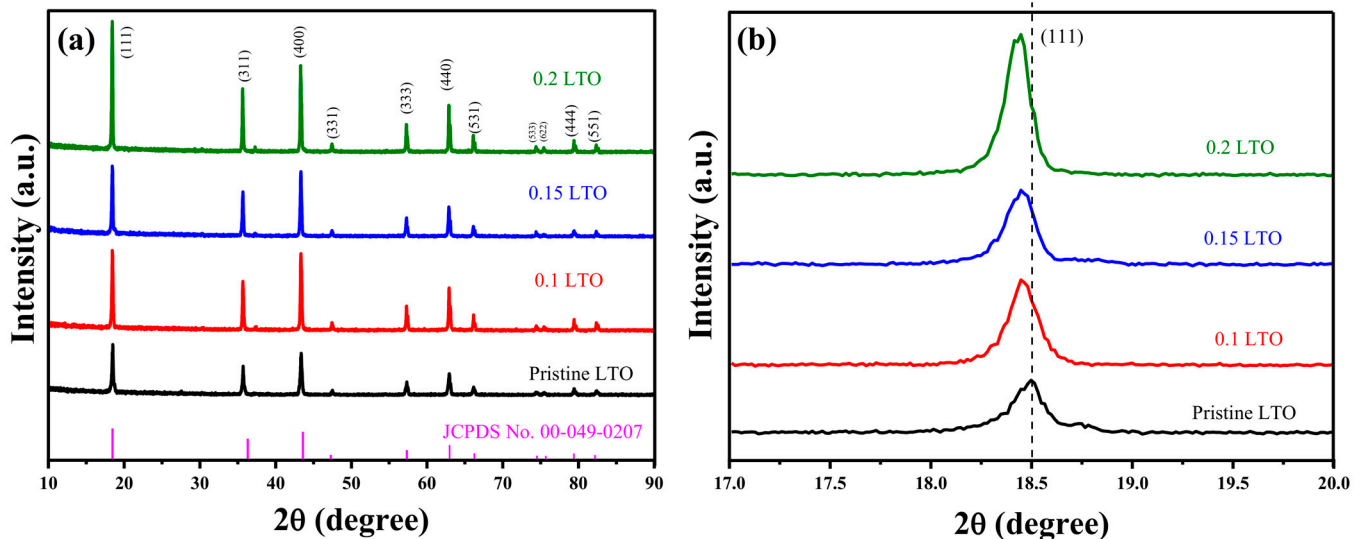


Figure 1. (a) XRD pattern of pristine and iodide-doped LTO and (b) magnification of (111) peaks of pristine LTO and iodide-doped LTO.

Although the doping of iodide does not change the spinel structure of LTO, it seems the diffraction peaks of iodide-doped LTO have shifted to a lower degree. For further observation, the peak position of (111) plane is magnified, as shown in Figure 1b. The fitting results of XRD patterns are shown in Table 1, presenting the lattice parameter and cell volume of pristine and iodide-doped LTO. It appears that the increasing amount of iodide has increased the lattice parameter and cell volume of LTO.

Table 1. Lattice parameter and cell volume of pristine and iodide-doped LTO.

Sample	Lattice Parameter a (Å)	Cell Volume (10^6 pm^3)
Pristine LTO	8.299	571.722
0.1 LTO	8.313	574.506
0.15 LTO	8.321	576.128
0.2 LTO	8.326	577.374

Figure 2a–d shows the morphology particles of the pristine LTO and iodide-doped LTO. Figure 2 depicts the irregular grain-shaped particles in all LTO samples (a–d). It is observed that some particles are of rectangular-like shape with big agglomeration. The particles are distributed randomly with interconnected grains. The grain size of iodide-doped LTO appears to be similar to that of pristine LTO. All grains are smaller than 1 μm , and some are smaller than 500 nanometers.

The distribution of each element on iodide-doped LTO is investigated by EDS mapping, as shown in Figure 3. It is clearly observed that the Ti, O, and I elements are evenly distributed on the surface of iodide-doped LTO. The iodide element really exists, even though the intensity is low.

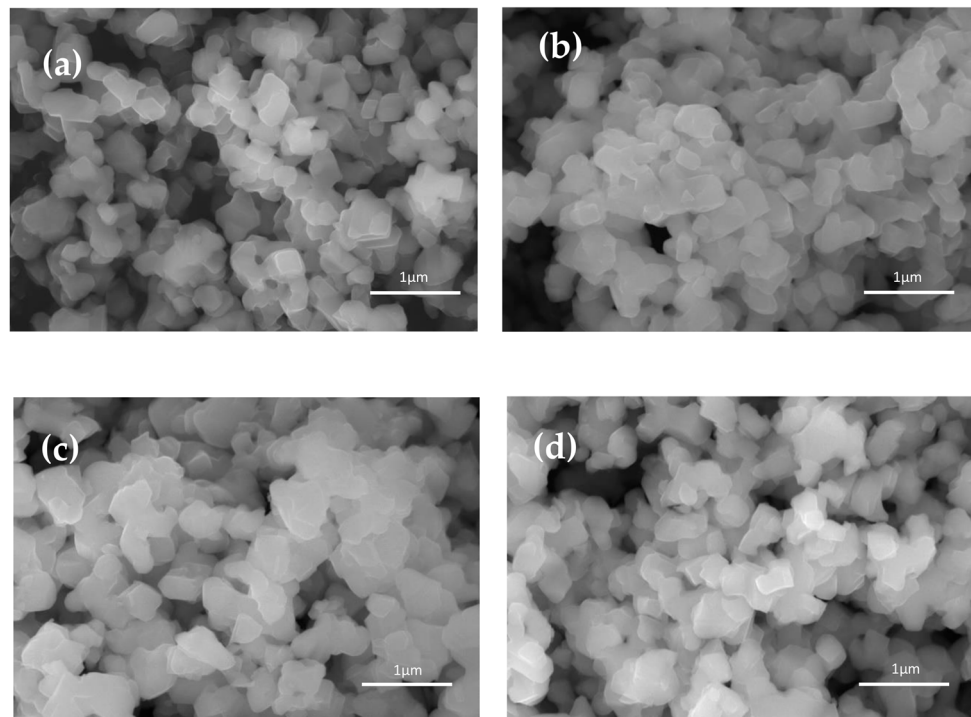


Figure 2. SEM images of (a) pristine LTO, (b) 0.1 LTO, (c) 0.15 LTO, and (d) 0.2 LTO.

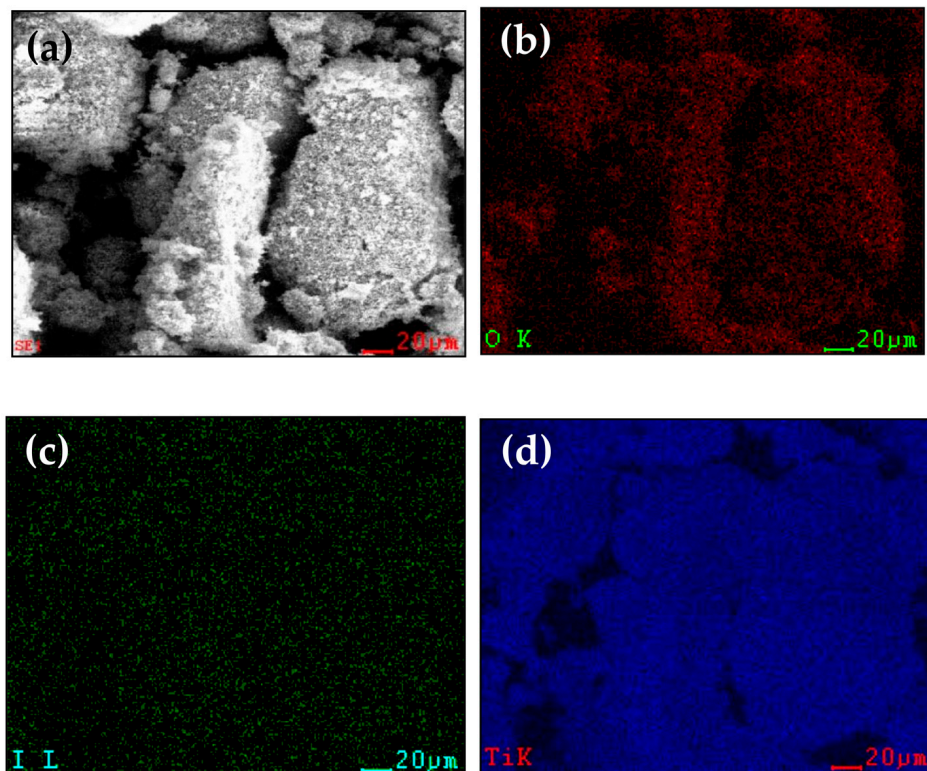


Figure 3. SEM/EDS images of 0.2 LTO; (a) images of 0.2 LTO, (b) O element, (c) I element, and (d) Ti element.

Figure 4 presents the electrochemical performance of pristine LTO and iodide-doped LTO. Figure 4a depicts the initial CV curve of all LTO samples in the potential window range of 0.75 to 2.75 V and a scan rate of 0.1 mV s^{-1} . It is clearly observed that individual LTO samples have a couple of redox peaks. The initial reduction curves of pristine LTO, 0.1 LTO,

0.15 LTO, and 0.2 LTO are located at 1.41, 1.42, 1.43, and 1.48 V, respectively, and can be associated with the intercalation process of Li ions into the spinel structure of $\text{Li}_4\text{Ti}_5\text{O}_{12}$ transferred to $\text{Li}_7\text{Ti}_5\text{O}_{12}$ [37]. Next, the oxidation (anodic) peaks in all CV curves overlap at 1.68, 1.70, 1.69, and 1.68 V, demonstrating the reversible process of electrochemical reactions in pristine LTO, 0.1 LTO, 0.15 LTO, and 0.2 LTO.

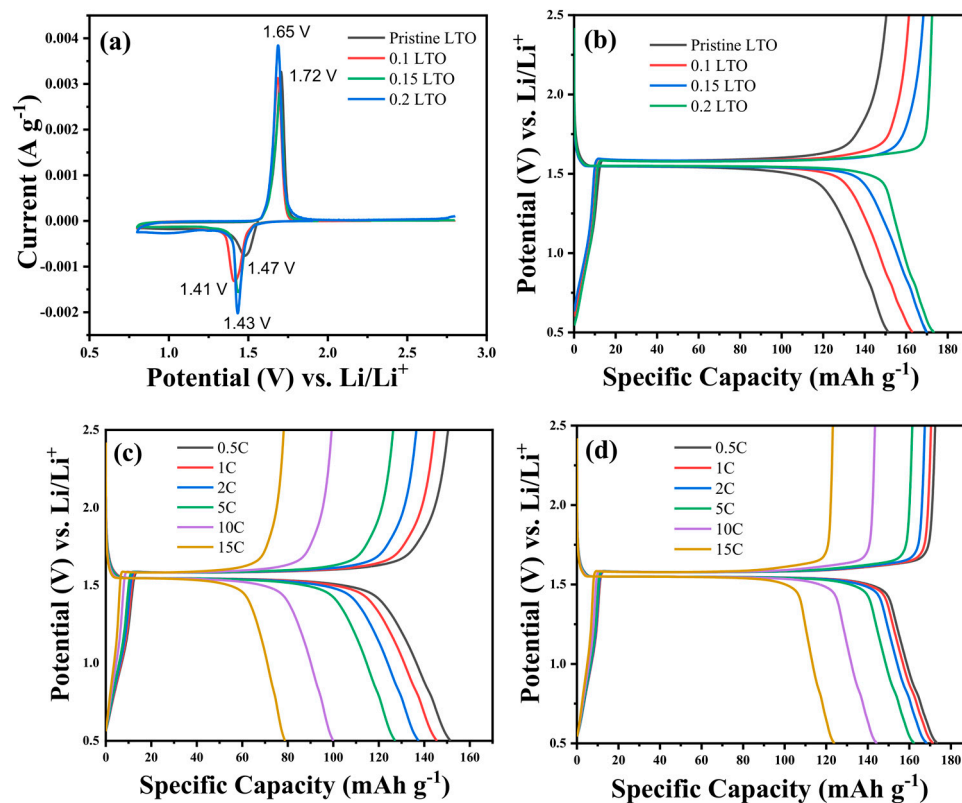


Figure 4. (a) Cyclic voltammetry of all LTO, (b) the charge–discharge profile for pristine LTO and iodide-doped LTO at 0.5C; the high-rate charge–discharge performance of (c) pristine LTO, and (d) 0.2 LTO.

Figure 4b displays the initial charge–discharge curves of pristine and iodide-doped LTO at 0.5C with the potential range of 0.5–2.5 V vs. Li^+/Li . A flat voltage plateau of about 1.52 V is observed for all LTO samples attributing to a typical character of LTO. The charge–discharge voltage plateau of 0.2 LTO is significantly longer than that of all LTO samples. From Figure 4b, it is determined that the pristine LTO has an initial specific discharge capacity of $151.46 \text{ mAh g}^{-1}$, 0.1 LTO ($162.28 \text{ mAh g}^{-1}$), 0.15 LTO ($169.67 \text{ mAh g}^{-1}$) and 0.2 LTO ($172.43 \text{ mAh g}^{-1}$). It is clear that 0.2 LTO has the most excellent initial specific discharge capacity, followed by 0.15 LTO, 0.1 LTO, and pristine LTO samples.

The initial charge–discharge profiles of pristine LTO and 0.2 LTO are shown in Figure 4c,d at varying current densities of 0.5, 1, 2, 5, 10, and 15 C. The charge–discharge curve decreases steadily as current density increases due to increased ohmic polarization and polarization concentration [37]. At currents of 0.5, 1, 2, 5, 10, and 15 C, respectively, the pristine LTO delivers specific discharge capacities of 151.46, 145.49, 137.54, 127.26, 99.29, and 78.82 mAh g^{-1} , whereas 0.2 LTO has specific discharge capacities of 172.43, 171.19, 167.42, 161.40, 143.45, and $123.31 \text{ mAh g}^{-1}$. These results verify that the specific discharge capacity of the 0.2 LTO sample in high-rate current density is greater than that of pristine LTO.

The comparison of the rate performance of the pristine LTO and iodide-doped LTO is shown in Figure 5a. All LTO samples demonstrated excellent rate and cyclic performance in the low current density due to the stable structure characteristic of LTO. However,

the gap in specific discharge capacity between LTO samples becomes more noticeable when the current density increases. The 0.2 LTO has higher specific discharge capacities of $123.31 \text{ mAh g}^{-1}$ with currents of 15 C compared to other LTO samples. The specific discharge capacity of other iodide-doped LTO at different rates lies between 0.2 LTO and pristine LTO. It is indicated that the rate performance of 0.2 LTO was enhanced by doping of iodide. Figure 5b presents the stable cyclic performance of 0.2 LTO with a specific discharge capacity of $171.19 \text{ mAh g}^{-1}$ at 1 C after 100 cycles. In general, 0.2 LTO has an excellent retention capacity of 99.15% compared to the other LTO samples (LTO 93.04%, 0.1 LTO 96.33%, and 0.15 LTO 98.12%) in the long-term cycling performance test.

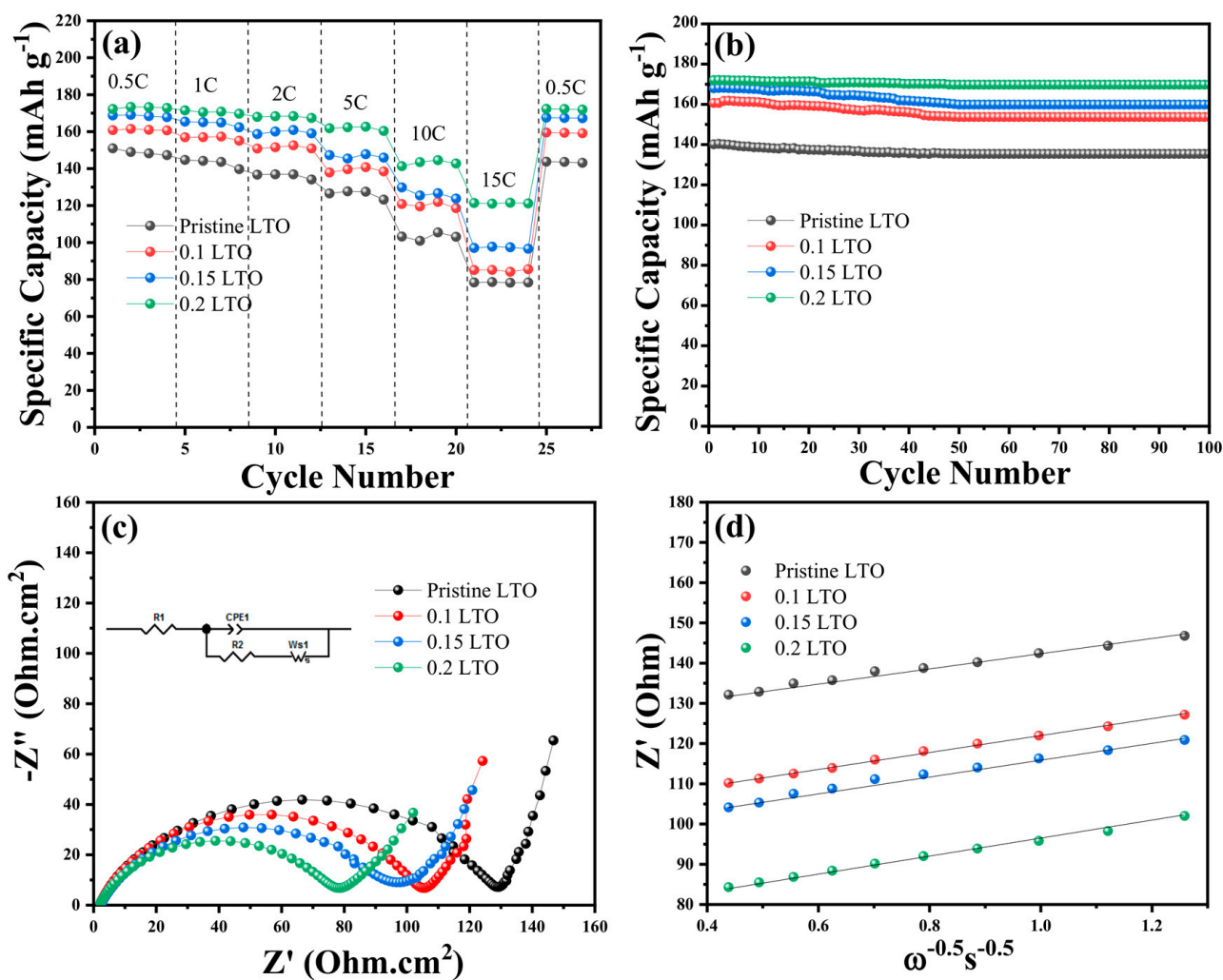


Figure 5. Electrochemical performance of pristine LTO and iodide-doped LTO: (a) capability in different current densities, (b) cyclic performance, (c) AC impedance spectra with an inserted equivalent circuit, and (d) Li⁺ diffusion plot-rate capability (a), cyclability (b), Nyquist plot with inserted equivalent circuit (c), and Li⁺ diffusion profile (d) of pristine LTO and LTO 0.2F.

The enhanced electrochemical performance of iodide-doped LTO was also investigated by electrochemical impedance spectroscopy (EIS), as seen in Figure 5c. Figure 5c depicts a Nyquist plot and an equivalent circuit with the resistance of the charge transfer process represented by the semicircle in the high-frequency region of the impedance curve and lithium diffusion by the inclined line intercept in the low frequency, respectively. In the equivalent circuit, where R1 or R_s represents the electrolyte, separator, and electrode resistance, R2 or R_{ct} is charge transfer resistance represented by a semicircle, CPE is an abbreviation of constant phase element and the Warburg impedance for sloping line at low frequencies. According to the fitting results, the R_{ct} of 0.2 LTO is $83.26 \Omega \cdot \text{cm}^{-2}$ less than

that of pristine ($134.95 \Omega \cdot \text{cm}^{-2}$) and other iodide-doped LTO (0.1 LTO $112.50 \Omega \cdot \text{cm}^{-2}$, and 0.15 LTO $104.13 \Omega \cdot \text{cm}^{-2}$). It demonstrates that the 0.2 LTO has a higher charge transfer capability and lower electrochemical polarization, resulting in a faster kinetic reaction of lithium ions. The improved electrochemical of 0.2 LTO was also supported by the calculation of the diffusion rate of Li (D) ions using the following equation [38,39]:

$$D = \frac{R^2 T^2}{2A^2 F^4 C_{\text{Li}}^2 \sigma^2} \quad (1)$$

The Warburg factor is calculated using the following formula:

$$Z_{\text{real}} = R_s + R_{\text{ct}} + (\sigma \omega^{-0.5}), \quad (2)$$

where detailed description D is the diffusion coefficient; R is gas constant; T is absolute temperature; A is the surface area of the electrode; F is Faraday's constant; C is the molar concentration of Li^+ ions; and ω is the angular frequency [40]. The diffusion coefficient is calculated from the curve in Figure 5d for pristine LTO, 0.1 LTO, 0.15 LTO, and 0.2 LTO is 8.97×10^{-14} , 2.10×10^{-13} , 3.35×10^{-13} , and $8.23 \times 10^{-12} \text{ cm}^{-2} \text{ s}^{-1}$, respectively. The 0.2 LTO has a higher diffusion lithium-ion coefficient.

To evaluate the morphology and microstructural integrity before and after cycling, the SEM analysis was conducted to observe the top surface and cross-section of the 0.2 LTO electrode. Figure 6a,b shows the top surface and cross-section of the 0.2 LTO electrode before and after the 100 cycling test. It is observed that the structural integrity of 0.2 LTO is maintained after 100 cycles without any significant degradation detected. This demonstrated that the stability and integrity of 0.2 LTO electrodes are well maintained during the cycling test even at high-current density. The present structure of 0.2 LTO is beneficial to prevent volume expansion and relieve the structure from damage during the cycling test.

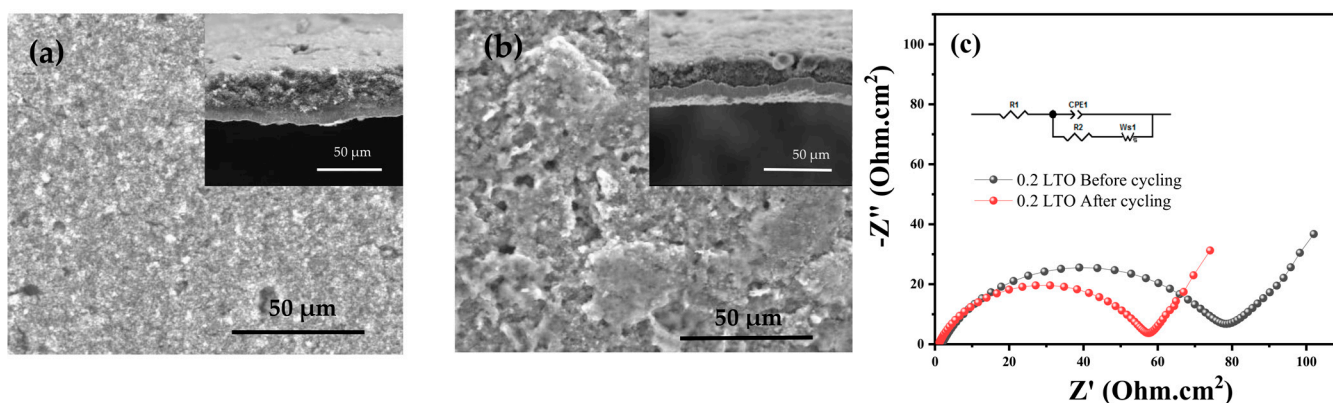


Figure 6. SEM images of iodide-doped LTO electrode: (a) before cycling with the insert of a cross-section of the electrode, (b) after cycling with the insert of cross-section of electrode, and (c) Nyquist plot with an inserted equivalent circuit.

Furthermore, the electronic conductivity and kinetic transfer of 0.2 LTO were evaluated by EIS measurement before and after 100 cycles as shown in Figure 6c. The spectra were fitted with a modified Randles equivalent circuit [41]. It is determined that the initial charge transfer resistance of 0.2 LTO is $83.26 \Omega \cdot \text{cm}^{-2}$ and that after cycling it decreased ($59.18 \Omega \cdot \text{cm}^{-2}$) compared to before cycling. It is attributed to the Li-ion effectively transferring and diffusing to the electrode/electrolyte interface [42].

3. Discussion

In all of the iodide-doped LTO samples, no impurity can be detected as seen in Figure 1. With increasing iodide doping, the intensity peaks of iodide-doped LTO increase. It is indicated that the iodide-doped LTO has a high degree of crystallinity. Although the doping

of iodide does not change the spinel structure of LTO, it seems the diffraction peaks of iodide-doped LTO have shifted to a lower degree. It appears that the increasing amount of iodide has increased the lattice parameter and cell volume of LTO. It is possible that the I^- ion taking the place of the O^{2-} ion causes the lattice parameter to increase. Ions of I^- have a larger ion size (0.206 nm) than those of O^{2-} (0.142 nm). This agrees with Vegard's substitutional principle [43]. As a result, the addition of I^- ion would increase the lattice parameter of iodide-doped LTO [44].

Compared to all LTO samples in cyclic voltammetry measurement presented in Figure 4a, the peak intensity of 0.2 LTO has the highest peak with a potential difference (0.22 V) that is less than that of other LTO samples, indicating that 0.2 LTO has a low polarization degree. It is demonstrated that iodide doping on LTO is useful for reducing electrode polarization. In addition, 0.2 LTO has the most significant redox peak current, indicating higher lithium storage and increasing the electronic conductivity performance [33].

It is clear that 0.2 LTO has the most excellent initial specific discharge capacity, followed by 0.15 LTO, 0.1 LTO, and pristine LTO samples as shown in Figure 4b. The higher initial discharge capacity of 0.2 LTO is most likely due to the addition of iodide doping to LTO that has contributed to increasing the conductivity. These results verify that the specific discharge capacity of the 0.2 LTO sample in high-rate current density is greater than that of pristine LTO. It is determined in Figure 4c,d that the polarization voltage as defining the difference between charge potential and discharge potential of 0.2 LTO is much lower than those of pristine LTO, which is implicated in the 0.2 LTO owing to higher reversible capacity compared to pristine LTO.

The 0.2 LTO has higher specific discharge capacities of 123.31 mAh g⁻¹ with currents of 15 C compared to other LTO samples. The specific discharge capacity of other iodide-doped LTO at different rates lies between 0.2 LTO and pristine LTO. It is indicated that the rate performance of 0.2 LTO was enhanced by doping of iodide. It can be because 0.2 LTO has a higher volume cell than pristine LTO as shown in Table 1. The increased crystal volume widens the paths for lithium ions to travel during insertion and extraction [45].

Figure 5c presents the fitting results of Nyquist plot; it is determined that the Rct of 0.2 LTO is 83.26 Ω.cm⁻² less than that of pristine (134.95 Ω.cm⁻²) and other iodide-doped LTOs (0.1 LTO 112.50 Ω.cm⁻², and 0.15 LTO 104.13 Ω.cm⁻²). It demonstrates that the 0.2 LTO has a higher charge transfer capability and lower electrochemical polarization, resulting in a faster kinetic reaction of lithium ions. The calculated results from Figure 5d show that the 0.2 LTO has a higher diffusion lithium-ion coefficient. It is demonstrated that iodide-doped LTO has enhanced the Li-ion diffusion capability and ionic conductivity. It can be a result of the bigger path opening in the spinel structure of 0.2 LTO (as shown in Table 1) for the transport of Li⁺ ions during the charging and discharging process.

In addition, Table 2 compares the electrochemical performance of the current iodide doping on the LTO with similar works. It shows that the 0.2 LTO has competitive electrochemical performance in terms of capacity and rate capability.

Table 2. Comparison of high-rate performance of the anion-doped LTO materials.

Material System	Synthesis Process	Voltage (V)	Discharge Capacity (mAh g ⁻¹)	High-Current Density	Ref.
Li ₄ Ti ₅ O _{12-x} F _x (x = 0.3)	Solid-state reaction	0.01–2.5	71.6	1700 mA g ⁻¹	[33]
Carbon-encapsulated F-doped Li ₄ Ti ₅ O ₁₂	Hydrothermal process and solid-state lithiation	1.0–3.0	123	10 C	[30]
Fluoride doping Li ₄ Ti ₅ O ₁₂ nanosheets	Hydrothermal process and calcination	0.5–2.5	131.9	2 A g ⁻¹	[29]
Li ₄ Ti ₅ O _{11.9} F _{0.1}	Solid-state reaction	1.0–3.0	99.2	10 C	[46]
Li ₄ Ti ₅ O _{11.7} F _{0.3}	Solid-state reaction	1.0–3.0	82	5 C	[43]
Iodide-doped Li ₄ Ti ₅ O ₁₂	Solid-state reaction	0.5–2.5	143	10 C	This work

4. Materials and Methods

4.1. Preparation of Double-Coated F-Doped LTO

Firstly, the pristine and Iodide-doped LTO were synthesized by using a solid-state method with a precursor of Li_2CO_3 (Merck, Darmstadt, Germany, 99%), TiO_2 (Merck, 99%), and LiI (Merck, 99%). The stoichiometric amount of all precursors was weighted and mixed based on 1 mol of LTO for preparation of pristine LTO, and iodide-doped LTO was prepared with 1 mol pristine LTO with the addition of 0.1, 0.15, and 0.2 mol of LiI . Then, 8 mL of 99% ethanol was added to the precursor powders in a ball mill chamber as a solvent. All powders were pulverized for six hours at 600 rpm in a high-energy ball mill with the zirconia type of ball for the milling process and the ball-to-powder ratio of 10:1. The powder mixture was dried and then heated to 750 °C for 10 h for calcination. Finally, pristine and iodide-doped LTO were obtained and assigned the following labels: pristine LTO, 0.1 LTO, 0.15 LTO, and 0.2 LTO.

4.2. Material Characterization

The phases of all samples were examined using an X-ray Diffraction (XRD) test using PANAnalytical (Phillips, Eindhoven, The Netherlands) at a 2θ angle ranging from 10° to 90° and $\text{CuK}\alpha$ wavelength of 1.54056 Å. The surface morphology and element distribution of iodide-doped LTO were observed by scanning electron microscopy and energy-dispersive X-ray spectroscopy SEM/EDS (Phillips-Inspect S50 FEI Technologies Inc., Hillsboro, OR, USA).

4.3. Electrochemical Measurement

The electrochemical performance testing of the half-cell system was conducted using a CR2032 coin cell. A glove box containing argon gas was used for the cell fabrication procedure (Vigor Tech, Houston, TX, USA). The electrode slurry was composed of an 80:10:10 weight ratio of active material, acetylene black, and polyvinylidene fluoride dissolved in *N*-methyl-2-pyrrolidinone (NMP). The slurry was then coated on the copper foil as a current collector before being dried for 12 h at 80 degrees in a vacuum oven. The electrode was prepared by cutting the coated copper foil into a circular form with a diameter of 1.2 mm and a loading mass of approximately 12 mg. Polypropylene micro-porous membrane (Celgard®, Charlotte, NC, USA) was used as a separator, and lithium metal as a counter electrode and reference electrode. The electrolyte for the test was prepared by dissolving 1 M LiPF_6 in ethyl methyl carbonate and ethylene carbonate solvents (7:3 volume ratio). Galvanostatic charge–discharge tests were carried out using the Neware CT-4008 (Neware Technology Limited, Shenzhen, China) instrument over a voltage range of 0.75–2.5 V with varying C-rates. Specific discharge capacity (C_{disch}) from Galvanostatic Charge–Discharge (GCD) for the battery was calculated with following equation:

$$C_{\text{disch}} = I\Delta t / (m), \quad (3)$$

where I is representative of current (A or mA), Δt is attributed to the period (h), and m signifies the active mass of the electrode (g).

Cyclic voltammetry (CV) test was performed using the CorrTest CS310 electrochemical workstation (Wuhan Corrttest Instruments Corp., Ltd., Wuhan, China) with a voltage range of 0.75–3.0 V vs. Li/Li^+ and a scan rate of 0.1 mV s^{-1} . The sample was tested using electrochemical impedance spectroscopy (EIS) over a frequency range of 0.1–100 kHz using the CorrTest CS310 electrochemical workstation.

5. Conclusions

The solid-state method was successfully carried out to synthesize iodide-doped LTO. The XRD results show that increasing the content of iodide has increased the lattice parameter of the LTO spinel structure without any impurities detected. The doping of iodide does not significantly impact the particle size and shape of LTO. In all, 0.2 LTO has the best

cyclic capability, with an initial specific discharge capacity of 171.19 mAh g⁻¹ and capacity fading of 99.15% at 1 C after 100 cycles. In addition, 0.2 LTO shows the best high-rate performance with a specific discharge capacity of 123.31 mAh g⁻¹ at 15 C. Furthermore, the 0.2 LTO has a low charge transfer resistance and higher diffusion lithium-ion coefficient. It is indicated that iodide-doped LTO has enhanced the Li-ion diffusion capability and ionic conductivity because of the more significant path opening in the crystal structure of 0.2 LTO as shown in XRD results. Therefore, in this work, doping iodide significantly enhances the electrochemical performance of LTO, which shows higher rate capability and excellent cycle performance.

Author Contributions: Conceptualization and writing—original draft, L.N.; methodology, A.S.; validation, D.S.; investigation, R.S.P.; resources, W.W.; writing—review and editing, N.H.I.; funding acquisition, L.N. All authors have read and agreed to the published version of the manuscript.

Funding: Ministry of Education and Culture was acknowledged for financial support through WCR 2022 scheme (No. 1601/PKS/ITS/2022).

Data Availability Statement: The data presented in this study are available on request from the corresponding author.

Conflicts of Interest: The authors declare no conflict of interest.

References

1. Zhao, B.; Ran, R.; Liu, M.; Shao, Z. A comprehensive review of Li₄Ti₅O₁₂-based electrodes for lithium-ion batteries: The latest advancements and future perspectives. *Mater. Sci. Eng. R Rep.* **2015**, *98*, 1–71. [[CrossRef](#)]
2. Fong, R.; von Sacken, U.; Dahn, J.R. Studies of Lithium Intercalation into Carbons Using Nonaqueous Electrochemical Cells. *J. Electrochem. Soc.* **1990**, *137*, 2009–2013. [[CrossRef](#)]
3. Bai, P.; Li, J.; Brushett, F.R.; Bazant, M.Z. Transition of lithium growth mechanisms in liquid electrolytes. *Energy Environ. Sci.* **2016**, *9*, 3221–3229. [[CrossRef](#)]
4. Wang, J.; Kober, D.; Shao, G.; Epping, J.D.; Görke, O.; Li, S.; Gurlo, A.; Bekheet, M.F. Stable anodes for lithium-ion batteries based on tin-containing silicon oxycarbonitride ceramic nanocomposites. *Mater. Today Energy* **2022**, *26*, 100989. [[CrossRef](#)]
5. Azam, M.A.; Safie, N.E.; Ahmad, A.S.; Yuza, N.A.; Zulkifli, N.S.A. Recent advances of silicon, carbon composites and tin oxide as new anode materials for lithium-ion battery: A comprehensive review. *J. Energy Storage* **2021**, *33*, 102096. [[CrossRef](#)]
6. Perumal, P.; Sivaraj, P.; Abhilash, K.P.; Soundarya, G.G.; Balraju, P.; Selvin, P.C. Green synthesized spinel lithium titanate nano anode material using Aloe Vera extract for potential application to lithium ion batteries. *J. Sci. Adv. Mater. Devices* **2020**, *5*, 346–353. [[CrossRef](#)]
7. Rabiei Baboukani, A.; Khakpour, I.; Drozd, V.; Wang, C. Liquid-Based Exfoliation of Black Phosphorus into Phosphorene and Its Application for Energy Storage Devices. *Small Struct.* **2021**, *2*, 2000148. [[CrossRef](#)]
8. Li, B.; Han, C.; He, Y.-B.; Yang, C.; Du, H.; Yang, Q.-H.; Kang, F. Facile synthesis of Li₄Ti₅O₁₂/C composite with super rate performance. *Energy Environ. Sci.* **2012**, *5*, 9595–9602. [[CrossRef](#)]
9. Kang, E.; Jung, Y.S.; Kim, G.-H.; Chun, J.; Wiesner, U.; Dillon, A.C.; Kim, J.K.; Lee, J. Highly Improved Rate Capability for a Lithium-Ion Battery Nano-Li₄Ti₅O₁₂ Negative Electrode via Carbon-Coated Mesoporous Uniform Pores with a Simple Self-Assembly Method. *Adv. Funct. Mater.* **2011**, *21*, 4349–4357. [[CrossRef](#)]
10. Wang, P.; Zhang, G.; Cheng, J.; You, Y.; Li, Y.-K.; Ding, C.; Gu, J.-J.; Zheng, X.-S.; Zhang, C.-F.; Cao, F.-F. Facile Synthesis of Carbon-Coated Spinel Li₄Ti₅O₁₂/Rutile-TiO₂ Composites as an Improved Anode Material in Full Lithium-Ion Batteries with LiFePO₄@N-Doped Carbon Cathode. *ACS Appl. Mater. Interfaces* **2017**, *9*, 6138–6143. [[CrossRef](#)]
11. Zhao, L.; Hu, Y.-S.; Li, H.; Wang, Z.; Chen, L. Porous Li₄Ti₅O₁₂ Coated with N-Doped Carbon from Ionic Liquids for Li-Ion Batteries. *Adv. Mater.* **2011**, *23*, 1385–1388. [[CrossRef](#)] [[PubMed](#)]
12. Mo, L.; Zheng, H. Solid coated Li₄Ti₅O₁₂ (LTO) using polyaniline (PANI) as anode materials for improving thermal safety for lithium ion battery. *Energy Rep.* **2020**, *6*, 2913–2918. [[CrossRef](#)]
13. Jang, I.-S.; Hui Kang, S.; Chan Kang, Y.; Roh, K.C.; Chun, J. Facile synthesis of surface fluorinated-Li₄Ti₅O₁₂/carbon nanotube nanocomposites for a high-rate capability anode of lithium-ion batteries. *Appl. Surf. Sci.* **2022**, *605*, 154710. [[CrossRef](#)]
14. Opra, D.P.; Gnedenkov, S.V.; Sinebryukhov, S.L. Recent efforts in design of TiO₂(B) anodes for high-rate lithium-ion batteries: A review. *J. Power Sources* **2019**, *442*, 227225. [[CrossRef](#)]
15. Liu, Y.; Wang, W.; Chen, J.; Li, X.; Cheng, Q.; Wang, G. Fabrication of porous lithium titanate self-supporting anode for high performance lithium-ion capacitor. *J. Energy Chem.* **2020**, *50*, 344–350. [[CrossRef](#)]
16. Qi, Y.; Huang, Y.; Jia, D.; Bao, S.-J.; Guo, Z.P. Preparation and characterization of novel spinel Li₄Ti₅O_{12-x}Br_x anode materials. *Electrochim. Acta* **2009**, *54*, 4772–4776. [[CrossRef](#)]
17. Jing, X.; Wang, Y.; Zhang, X.; Lang, J.; Wang, W. Anchoring nitrogen-doped carbon particles on lithium titanate to enhance its lithium storage performance. *J. Electroanal. Chem.* **2020**, *871*, 114293. [[CrossRef](#)]

18. Zhang, Q.; Zhang, C.; Li, B.; Kang, S.; Li, X.; Wang, Y. Preparation and electrochemical properties of Ca-doped $\text{Li}_4\text{Ti}_5\text{O}_{12}$ as anode materials in lithium-ion battery. *Electrochim. Acta* **2013**, *98*, 146–152. [[CrossRef](#)]
19. Zhang, Q.; Zhang, C.; Li, B.; Jiang, D.; Kang, S.; Li, X.; Wang, Y. Preparation and characterization of W-doped $\text{Li}_4\text{Ti}_5\text{O}_{12}$ anode material for enhancing the high rate performance. *Electrochim. Acta* **2013**, *107*, 139–146. [[CrossRef](#)]
20. Wang, W.; Jiang, B.; Xiong, W.; Wang, Z.; Jiao, S. A nanoparticle Mg-doped $\text{Li}_4\text{Ti}_5\text{O}_{12}$ for high rate lithium-ion batteries. *Electrochim. Acta* **2013**, *114*, 198–204. [[CrossRef](#)]
21. Wang, D.; Zhang, C.; Zhang, Y.; Wang, J.; He, D. Synthesis and electrochemical properties of La-doped $\text{Li}_4\text{Ti}_5\text{O}_{12}$ as anode material for Li-ion battery. *Ceram. Int.* **2013**, *39*, 5145–5149. [[CrossRef](#)]
22. Zhang, Z.; Cao, L.; Huang, J.; Zhou, S.; Huang, Y.; Cai, Y. Hydrothermal synthesis of Zn-doped $\text{Li}_4\text{Ti}_5\text{O}_{12}$ with improved high rate properties for lithium ion batteries. *Ceram. Int.* **2013**, *39*, 6139–6143. [[CrossRef](#)]
23. Liu, Z.; Sun, L.; Yang, W.; Yang, J.; Han, S.; Chen, D.; Liu, Y.; Liu, X. The synergic effects of Na and K co-doping on the crystal structure and electrochemical properties of $\text{Li}_4\text{Ti}_5\text{O}_{12}$ as anode material for lithium ion battery. *Solid State Sci.* **2015**, *44*, 39–44. [[CrossRef](#)]
24. Deng, X.; Li, W.; Zhu, M.; Xiong, D.; He, M. Synthesis of Cu-doped $\text{Li}_4\text{Ti}_5\text{O}_{12}$ anode materials with a porous structure for advanced electrochemical energy storage: Lithium-ion batteries. *Solid State Ion.* **2021**, *364*, 115614. [[CrossRef](#)]
25. Zou, S.; Wang, G.; Zhang, Y.; Xue, C.; Chen, H.; Yang, G.; Nan, H.; Wei, H.; Lin, H. Nano-structure and characterization of carbon composite with Al^{3+} and Mn^{4+} co-doped $\text{Li}_4\text{Ti}_5\text{O}_{12}$ as anodes for Li-ion batteries. *J. Alloys Compd.* **2020**, *816*, 152609. [[CrossRef](#)]
26. Meng, Q.; Chen, F.; Hao, Q.; Li, N.; Sun, X. Nb-doped $\text{Li}_4\text{Ti}_5\text{O}_{12}$ - TiO_2 hierarchical microspheres as anode materials for high-performance Li-ion batteries at low temperature. *J. Alloys Compd.* **2021**, *885*, 160842. [[CrossRef](#)]
27. Gong, S.H.; Lee, J.H.; Chun, D.W.; Bae, J.-H.; Kim, S.-C.; Yu, S.; Nahm, S.; Kim, H.-S. Effects of Cr doping on structural and electrochemical properties of $\text{Li}_4\text{Ti}_5\text{O}_{12}$ nanostructure for sodium-ion battery anode. *J. Energy Chem.* **2021**, *59*, 465–472. [[CrossRef](#)]
28. Ruiyi, L.; Yuanyuan, J.; Xiaoyan, Z.; Zaijun, L.; Zhiguo, G.; Guangli, W.; Junkang, L. Significantly enhanced electrochemical performance of lithium titanate anode for lithium ion battery by the hybrid of nitrogen and sulfur co-doped graphene quantum dots. *Electrochim. Acta* **2015**, *178*, 303–311. [[CrossRef](#)]
29. Chen, Y.; Qian, C.; Zhang, P.; Zhao, R.; Lu, J.; Chen, M. Fluoride doping $\text{Li}_4\text{Ti}_5\text{O}_{12}$ nanosheets as anode materials for enhanced rate performance of lithium-ion batteries. *J. Electroanal. Chem.* **2018**, *815*, 123–129. [[CrossRef](#)]
30. Ma, Y.; Ding, B.; Ji, G.; Lee, J.Y. Carbon-Encapsulated F-Doped $\text{Li}_4\text{Ti}_5\text{O}_{12}$ as a High Rate Anode Material for Li^+ Batteries. *ACS Nano* **2013**, *7*, 10870–10878. [[CrossRef](#)]
31. Zhang, Q.; Lu, H.; Zhong, H.; Yan, X.; Ouyang, C.; Zhang, L. W^{6+} & Br^- codoped $\text{Li}_4\text{Ti}_5\text{O}_{12}$ anode with super rate performance for Li-ion batteries. *J. Mater. Chem. A* **2015**, *3*, 13706–13716. [[CrossRef](#)]
32. Noerochim, L.; Wibowo, A.T.; Widyastuti; Subhan, A.; Prihandoko, B.; Caesarendra, W. Direct Double Coating of Carbon and Nitrogen on Fluoride-Doped $\text{Li}_4\text{Ti}_5\text{O}_{12}$ as an Anode for Lithium-Ion Batteries. *Batteries* **2022**, *8*, 5. [[CrossRef](#)]
33. Zhao, Z.; Xu, Y.; Ji, M.; Zhang, H. Synthesis and electrochemical performance of F-doped $\text{Li}_4\text{Ti}_5\text{O}_{12}$ for lithium-ion batteries. *Electrochim. Acta* **2013**, *109*, 645–650. [[CrossRef](#)]
34. Su, W.; Zhang, Y.; Li, Z.; Wu, L.; Wang, X.; Li, J.; Fu, X. Multivalency Iodine Doped TiO_2 : Preparation, Characterization, Theoretical Studies, and Visible-Light Photocatalysis. *Langmuir* **2008**, *24*, 3422–3428. [[CrossRef](#)]
35. Zhao, Y.; Wei, J.; Vajtai, R.; Ajayan, P.M.; Barrera, E. V Iodine doped carbon nanotube cables exceeding specific electrical conductivity of metals. *Sci. Rep.* **2011**, *1*, 83. [[CrossRef](#)] [[PubMed](#)]
36. Ameen, S.; Song, M.; Kim, D.-G.; Im, Y.-B.; Seo, H.-K.; Kim, Y.S.; Shin, H.-S. Iodine doped polyaniline thin film for heterostructure devices via PECVD technique: Morphological, structural, and electrical properties. *Macromol. Res.* **2012**, *20*, 30–36. [[CrossRef](#)]
37. Yuan, T.; Cai, R.; Wang, K.; Ran, R.; Liu, S.; Shao, Z. Combustion synthesis of high-performance $\text{Li}_4\text{Ti}_5\text{O}_{12}$ for secondary Li-ion battery. *Ceram. Int.* **2009**, *35*, 1757–1768. [[CrossRef](#)]
38. Shu, H.; Wang, X.; Wu, Q.; Ju, B.; Liu, L.; Yang, X.; Wang, Y.; Bai, Y.; Yang, S. Ammonia Assisted Hydrothermal Synthesis of Monodisperse LiFePO_4/C Microspheres as Cathode Material for Lithium Ion Batteries. *J. Electrochem. Soc.* **2011**, *158*, A1448–A1454. [[CrossRef](#)]
39. Qian, D.; Gu, Y.; Chen, Y.; Liu, H.; Wang, J.; Zhou, H. Ultra-high specific capacity of Cr^{3+} -doped $\text{Li}_4\text{Ti}_5\text{O}_{12}$ at 1.55 V as anode material for lithium-ion batteries. *Mater. Lett.* **2019**, *238*, 102–106. [[CrossRef](#)]
40. Noerochim, L.; Caesarendra, W.; Habib, A.; Widyastuti; Suwarno; Ni'mah, Y.L.; Subhan, A.; Prihandoko, B.; Kosasih, B. Role of TiO_2 Phase Composition Tuned by LiOH on The Electrochemical Performance of Dual-Phase $\text{Li}_4\text{Ti}_5\text{O}_{12}$ - TiO_2 Microrod as an Anode for Lithium-Ion Battery. *Energies* **2020**, *13*, 5251. [[CrossRef](#)]
41. Rabiei Baboukani, A.; Khakpour, I.; Adelowo, E.; Drozd, V.; Shang, W.; Wang, C. High-performance red phosphorus-sulfurized polyacrylonitrile composite by electrostatic spray deposition for lithium-ion batteries. *Electrochim. Acta* **2020**, *345*, 136227. [[CrossRef](#)]
42. Jadhav, H.S.; Pawar, S.M.; Jadhav, A.H.; Thorat, G.M.; Seo, J.G. Hierarchical Mesoporous 3D Flower-like $\text{CuCo}_2\text{O}_4/\text{NF}$ for High-Performance Electrochemical Energy Storage. *Sci. Rep.* **2016**, *6*, 31120. [[CrossRef](#)]
43. Kahrizi, M.; Ghaffarinejad, A.; Daneshlab, R. Preparation and effects of F-doping on electrochemical properties of $\text{Li}_4\text{Ti}_5\text{O}_{12}$ as anode material for Li-ion battery. *Ionics* **2021**, *27*, 1929–1937. [[CrossRef](#)]
44. Scharner, S.; Weppner, W.; Schmid-Beurmann, P. Evidence of Two-Phase Formation upon Lithium Insertion into the $\text{Li}_{1.33}\text{Ti}_{1.67}\text{O}_4$ Spinel. *J. Electrochem. Soc.* **1999**, *146*, 857–861. [[CrossRef](#)]

45. Tsai, P.; Nasara, R.N.; Shen, Y.; Liang, C.; Chang, Y.; Hsu, W.-D.; Thuy Tran, N.T.; Lin, S. Ab initio phase stability and electronic conductivity of the doped- $\text{Li}_4\text{Ti}_5\text{O}_{12}$ anode for Li-ion batteries. *Acta Mater.* **2019**, *175*, 196–205. [[CrossRef](#)]
46. Bai, X.; Li, W.; Wei, A.; Chang, Q.; Zhang, L.; Liu, Z. Preparation and electrochemical performance of F-doped $\text{Li}_4\text{Ti}_5\text{O}_{12}$ for use in the lithium-ion batteries. *Solid State Ion.* **2018**, *324*, 13–19. [[CrossRef](#)]

Disclaimer/Publisher’s Note: The statements, opinions and data contained in all publications are solely those of the individual author(s) and contributor(s) and not of MDPI and/or the editor(s). MDPI and/or the editor(s) disclaim responsibility for any injury to people or property resulting from any ideas, methods, instructions or products referred to in the content.